Title

Over 67 GHz bandwidth hybrid silicon electroabsorption modulator with asymmetric segmented electrode for 1.3 μm transmission

Journal

Optics Express, 20(10)

Authors

Tang, Yongbo
Peters, Jonathan
Bowers, John E

Publication Date

2012-05-04

Over 67 GHz bandwidth hybrid silicon electroabsorption modulator with asymmetric segmented electrode for 1.3 μm transmission

Yongbo Tang,* Jonathan D. Peters, and John E. Bowers

Department of Electrical and Computer Engineering, University of California Santa Barbara, Santa Barbara, CA 93106, USA

ytang@ece.ucsb.edu

Abstract: A distributed III-V-on-Si electroabsorption modulator based on an asymmetric segmented electrode has been developed on the hybrid silicon platform for the 1.3 μm transmission window. The measured modulation response shows a 2 dB drop at 67 GHz and an extrapolated 3 dB bandwidth of 74 GHz. Large signal measurements show clearly open eye diagrams at 50 Gb/s. An extinction ratio of 9.6 dB for back to back transmission and an extinction ratio of 9.4 dB after 16 km transmission were obtained with a drive voltage of 2.2 V.

OCIS codes: (250.4110) Modulators; (250.5300) Photonic integrated circuits; (250.7360) Waveguide modulators.

References and links

1. D. A. Miller, "Rationale and challenges for optical interconnects to electronic chips," Proc. IEEE **88**(6), 728–749 (2000).
2. Z. Jia, J. Yu, A. Chowdhury, G. Ellinas, and G.-K. Chang, "Simultaneous generation of independent wired and wireless services using a single modulator in millimeter-wave-band Radio-Over-Fiber systems," IEEE Photon. Technol. Lett. **19**(20), 1691–1693 (2007).
3. X. S. Yao and L. Maleki, "Optoelectronic microwave oscillator," J. Opt. Soc. Am. B **13**(8), 1725–1735 (1996).
4. D. Thomson, F. Gardes, J.-M. Fedeli, S. Zlatanovic, Y. Hu, B. Kuo, E. Myslivets, N. Alic, S. Radic, G. Mashanovich, and G. Reed, "50-Gb/s silicon optical modulator," IEEE Photon. Technol. Lett. **24**(4), 234–236 (2012).
5. N.-N. Feng, D. Feng, S. Liao, X. Wang, P. Dong, H. Liang, C.-C. Kung, W. Qian, J. Fong, R. Shafiiha, Y. Luo, J. Cunningham, A. V. Krishnamoorthy, and M. Asghari, "30GHz Ge electro-absorption modulator integrated with 3 μm silicon-on-insulator waveguide," Opt. Express **19**(8), 7062–7067 (2011).
6. L. Alloatti, D. Korn, R. Palmer, D. Hillerkuss, J. Li, A. Barklund, R. Dinu, J. Wieland, M. Fournier, J. Fedeli, H. Yu, W. Bogaerts, P. Dumon, R. Baets, C. Koos, W. Freude, and J. Leuthold, "42.7 Gbit/s electro-optic modulator in silicon technology," Opt. Express **19**(12), 11841–11851 (2011).
7. M. Liu, X. Yin, E. Ulin-Avila, B. Geng, T. Zentgraf, L. Ju, F. Wang, and X. Zhang, "A graphene-based broadband optical modulator," Nature **474**(7349), 64–67 (2011).
8. Y. Tang, H.-W. Chen, S. Jain, J. D. Peters, U. Westergren, and J. E. Bowers, "50 Gb/s hybrid silicon traveling-wave electroabsorption modulator," Opt. Express **19**(7), 5811–5816 (2011).
9. D. Liang and J. Bowers, "Recent progress in lasers on silicon," Nat. Photonics **4**(8), 511–517 (2010).
10. H. H. Chang, Y. H. Kuo, R. Jones, A. Barkai, and J. E. Bowers, "Integrated hybrid silicon triplexer," Opt. Express **18**(23), 23891–23899 (2010).
11. M. Chacinski, U. Westergren, L. Thylen, B. Stoltz, J. Rosenzweig, R. Driad, R. E. Makon, J. Li, and A. Steffan, "ETDM Transmitter Module for 100-Gb/s Ethernet," IEEE Photon. Technol. Lett. **22**(2), 70–72 (2010).
12. T. Fujisawa, K. Takahata, W. Kobayashi, T. Tadokoro, N. Fujiwara, S. Kanazawa, and F. Kano, "1.3 μm, 50 Gbit/s electroabsorption modulators integrated with DFB laser for beyond 100G parallel LAN applications," Electron. Lett. **47**(12), 708–710 (2011).
13. T. Tatsumi, K. Tanaka, S. Sawada, H. Fujita, and T. Abe, "1.3 μm, 56-Gbit/s EML Module target to 400GbE," in Optical Fiber Communication Conference, OSA Technical Digest (Optical Society of America, 2012), paper OTh3F.4.
14. M. Shirai, H. Arimoto, K. Watanabe, A. Taike, K. Shinoda, J. Shimizu, H. Sato, T. Ido, T. Tsuchiya, M. Aoki, S. Tsuji, N. Sasada, S. Tada, and M. Okayasu, "40 Gbit/s electroabsorption modulators with impedance-controlled electrodes," Electron. Lett. **39**(9), 733–735 (2003).
15. R. Lewén, S. Irmscher, U. Westergren, L. Thylén, and U. Eriksson, "Segmented transmission-line electroabsorption modulators," J. Lightwave Technol. **22**(1), 172–179 (2004).

#165067 - $15.00 USD Received 21 Mar 2012; revised 26 Apr 2012; accepted 26 Apr 2012; published 4 May 2012

16. Y. Tang, Y. Yu, Y. Ye, U. Westergren, and S. He, "Design and optimization of an arbitrarily segmented traveling wave electrode for an ultrahigh speed electroabsorption modulator," Opt. Commun. **281**(20), 5177–5182 (2008).
17. D. Liang, G. Roelkens, R. Baets, and J. Bowers, "Hybrid integrated platforms for silicon photonics," Materials **3**(3), 1782–1802 (2010).

1. Introduction

Silicon photonics is an interesting research direction due to the possibility of high quality, low cost and high volume production of photonic integrated circuits (PICs) in CMOS foundaries, as well as the potential for low power, high capacity interconnects on future electronic-photonic integrated circuits (EPICs).

Pushing silicon PICs to a higher speed is desirable for many applications that need large capacity data transmission (e.g. high speed, low power consumption optical interconnects [1]) or long distance delivery of the microwave signal (e.g. radio-over-fiber link enabled milimeter-wave communication [2] and the optoelectronic oscillators for low phase noise microwave generation [3]). However, it is a challenge to realize a high speed and high efficiency modulator on the silicon platform. Manipulating the carrier concentration in silicon by carrier depletion can offer a fast but weak phase tuning and recently 50 Gb/s operation based on this machnism has been demonstrated with limited extinction ratio [4]. Alternative approaches based on Ge [5], polymer [6] and graphene [7] etc. have also been proposed on silicon-on-insulator (SOI) wafers and show potential ability for modulation beyond 50 Gb/s. To date the highest speed modulators on silicon were achieved by transferring a III-V epitaxy stack to an SOI wafer to realize a hybrid silicon electroabsorption modulator with 42 GHz bandwidth [8]. More importantly, with this hybrid silicon technique, the hybrid silicon modulator can be integrated with high performance semiconductor lasers [9] and high speed photodetectors [10], and hence enable the feasibility of complex on-chip photonic submodules and systems on silicon substrates, e.g., the hybrid silicon transmitter, similar to those developed on the InP substrate [11–13].

In this paper, we will report a distributed hybrid silicon modulator designed for a higher speed and a longer transmission distance. The improvement mainly comes from two aspects: first, an asymmetric segmented transmission line has been designed as the distributed electrode configuration [11, 14–16] to reduce the microwave reflection and improve the modulation bandwidth; second, we utilize a new InAlGaAs quantum well stack and shift the operation wavelength of the modulator to the 1.3 μm transmission window for datacom applications.

2. Device design and structure

2.1. Epitaxy

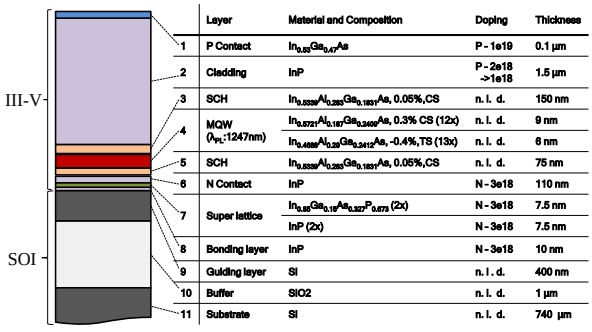

	Layer	Material and Composition	Doping	Thickness
1	P Contact	$In_{0.53}Ga_{0.47}As$	P - 1e19	0.1 μm
2	Cladding	InP	P - 2e18 ->1e18	1.5 μm
3	SCH	$In_{0.5539}Al_{0.2931}Ga_{0.1531}As$, 0.05%,CS	n. i. d.	150 nm
4	MQW (λ_{PL}:1247nm)	$In_{0.5721}Al_{0.197}Ga_{0.2409}As$, 0.3% CS (12x)	n. i. d.	9 nm
		$In_{0.4688}Al_{0.29}Ga_{0.2412}As$, -0.4%,TS (13x)	n. i. d.	6 nm
5	SCH	$In_{0.5539}Al_{0.2931}Ga_{0.1531}As$, 0.05%,CS	n. i. d.	75 nm
6	N Contact	InP	N - 3e18	110 nm
7	Super lattice	$In_{0.66}Ga_{0.19}As_{0.327}P_{0.673}$ (2x)	N - 3e18	7.5 nm
		InP (2x)	N - 3e18	7.5 nm
8	Bonding layer	InP	N - 3e18	10 nm
9	Guiding layer	SI	n. i. d.	400 nm
10	Buffer	SiO2	n. i. d.	1 μm
11	Substrate	SI	n. i. d.	740 μm

Fig. 1. Detailed structures of the III-V epitaxy stack and the SOI wafer.

The hybrid silicon electroabsorption modulator (HSEAM) uses a III-V epitaxy stack originally grown on an InP substrate that is transferred to a pre-patterned SOI wafer by O_2

#165067 - $15.00 USD Received 21 Mar 2012; revised 26 Apr 2012; accepted 26 Apr 2012; published 4 May 2012

plasma-assisted low temperature wafer bonding technique [17]. Figure 1 shows the detailed structure of the III-V epitaxy stack and the SOI wafer used for our fabrication. We chose offset InAlGaAs/InAlGaAs multiple quantum wells (MQWs) (offset relative to the silicon guiding layer) as the absorption medium. The InAlGaAs MQWs, due to its larger bandgap offset compared with InGaAsP MQWs, gives a stronger quantum confined Stark effect (QCSE) and hence a better modulation efficiency. The MQWs contain 12 compressive-strained wells and 13 tensile-strain-compensated barriers, with a total thickness of 186 nm. It is designed for transvese electric (TE) polarization, compatible with conventional semiconductor diode lasers. The photoluminescence (PL) peak of the MQWs has been shifted to 1247 nm by tuning the compositions of the MQW. This configuration allows the modulator to work in the 1.3 μm transmission window. We also applied a gradual-doping profile of 2e18 to 1e18 to the p-InP cladding layer in order to reduce the series resistance. The SOI wafer consists of a 400 nm guiding silicon layer, a 1 μm oxide layer and a 725 μm thick silicon substrate. We use a substrate with a high resistivity of 1000 Ω·cm for small microwave loss.

2.2. Electrode

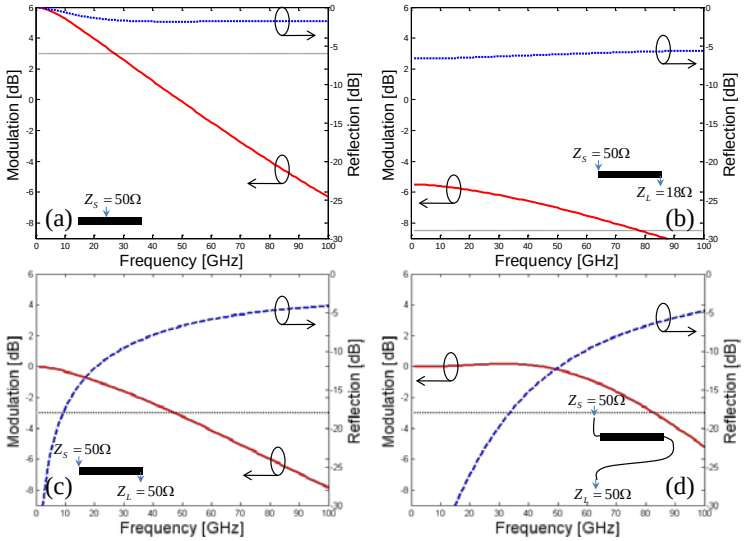

Fig. 2. Calculated modulation responses and reflections for 100μm long modulators using (a) a lumped electrode, (b) a traveling-wave electrode with a matched load of 18 Ω, (c) a traveling-wave electrode with a 50 Ω load and (d) a segmented electrode with a 50 Ω load. The insets show the schematics of the electrode configurations.

The electrode design is very important for an electroabsorption modulator. It will affect the modulation bandwidth, the microwave reflection and the modulation efficiency (via the voltage across the intrinsic junction). Figure 2 shows the calculated modulation responses and the reflections for four modulator designs with different electrode configurations based on a common 100 μm active modulation segment. The calculations are based on a transmission-matrix-based model as derived in [16] for a general distributed electrode and a lumped electrode with an open end is equivalent to a distributed case terminated by an infinite load. As shown in Fig. 2, the lumped electrode gives the best modulation efficiency since the forward voltage and the reflection at the open end are added constructively and give a double total voltage compared with that with a matched load. However, the bandwidth of a lumped EAM is seriously limited by the RC penalty, where C is mainly the intrinsic capacitance and R includes both the series resistance and the source impedance. Using a distributed electrode with a load Z_L at the end, the part of the RC related with the source impedance Z_S will be eliminated and the bandwidth can be greatly increased. If Z_L equals the characteristic

#165067 - $15.00 USD Received 21 Mar 2012; revised 26 Apr 2012; accepted 26 Apr 2012; published 4 May 2012

impedance Z_m of the active segment, the impedance matching at the end of the active segment can be achieved and leads to a real 'traveling-wave' (TW) operation with no reflection coming back to the active segment from the load. However, for a preferable active structure, Z_m is usually less than 25 Ω and in our case it is only 18 Ω. The TW operation requires a non-standard low value load to match Z_m. As shown in Fig. 2(b), it shows an obvious drop of the modulation efficiency in the low frequency range and significant reflection back to the source across the useful frequency range. Simply replacing the low value terminator by a standard 50 Ω load as shown in Fig. 2(c) can improve both the low modulation efficiency and the reflection in the low frequency range, however, at the expense of a reduced bandwidth (while it is still much larger than the bandwidth of the lumped configuration) [8].

A segmented electrode with low impedance active modulation segments and high impedance passive transmission line (TL) segments being alternately cascaded emerges to be a better method regarding the overall consideration of the modulation bandwidth, the microwave reflection and the modulation efficiency. The segmented electrode was first proposed as an impedance-controlled electrode in [14] and then extended to the case with multiple active segments in [15]. Here, due to the use of a short active length, we use the configuration with only one active segment to avoid additional optical loss [15]. The benefits of this segmented electrode come from the freedom of tuning the lengths of the passive TL segments and also the use of a standard 50 Ω load. As shown in Fig. 2(d), a well-designed segmented electrode can achieve a wideband impedance match at the input port and gives a flat feed-in efficiency across a large frequency range. The segmented configuration with a low impedance TL segment being sandwitched by two high impedance TL segments also introduce a positive 'standing-wave' effect in the low impedance region where the reflected microwave is constructively added to the forward microwave, leading to an enhanced drive voltage. When this enhancement is tuned to appear at a high frequency range, it can compensate the roll-off of the modulation response and extend the modulation bandwidth significantly.

2.3. Structure

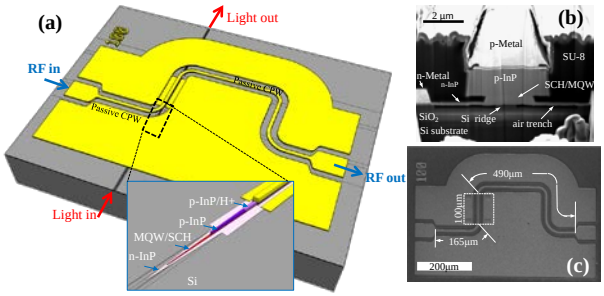

Fig. 3. (a) Schematic of a distributed HSEAM. Inset: enlarged taper part without the probe. (b) Cross section of the modulation waveguide. It was exposed by an ion focused beam and the SEM image was taken with a 52þ tilt angle. (c) Top-view SEM image of a final sample.

Figure 3 shows the schematic structure of our distributed HSEAM, as well as the SEM figures of the cross-section of the modulation segment and the top-vew of the final device. We employed an asymetric segmented electrode consisting of a 100μm-long active segment, a 165μm-long passive TL segment on the input side and another 490μm-long passive TL segment on the output side. The cross section of the active segment is shown in Fig. 2(b). An undercut process based on selectively wet etching has been adopted to narrow the intrisic layer to a width of around 2.35 μm while keeping the p-InP mesa width of 4 μm as defined by dry etching. A small silicon ridge width of 1 μm was chosen and the main part of the optical mode is confined in the intrinsic region, giving a confinement factor of 24% in the wells. The optical input and output are through the silicon waveguide and 70 μm long multi-level tapers

#165067 - $15.00 USD Received 21 Mar 2012; revised 26 Apr 2012; accepted 26 Apr 2012; published 4 May 2012

(see the inset of Fig. 3(a)) are used for the mode transition. The active segment has a characteristic impedance of around 18 Ω. Low loss coplanar waveguides (CPWs) with a high impedance of around 90 Ω are used as the passive TL segments. The strip width and the gap width of the CPW are 8 μm and 15 μm, respectively. Compared with the microstrip used in [11, 15], the CPW offers the flexibility of the control of the impedance based on the metal pattern (up to the mask and the lithography accuray) rather than the thickness of the dielectric layer (up to the process accuracy). Furthermore, the CPW design moves most of the metal to the top surface of the dielectric layer and hence empties the space underneath for the photonic components. We picked up the lengths of the CPWs based on an optimization procedure as described in [16] for a maximal modulation bandwidth. The final asymmetric configuration reflects the influence of the microwave loss due to the passive CPWs, i.e., the fact that only the loss of the input CPW will reduce the drive voltage on the modulation segment.

3. Device characteristics

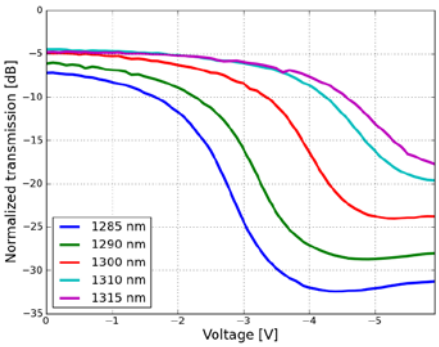

Fig. 4. Bias dependent transmission curves at different input wavelengths.

Figure 4 shows the measured transmission curves as a function of the bias at different input wavelengths. The data is normalized by the insertion loss of a reference silicon waveguide. The insertion loss of the modulator is around 4.9 dB for a wavelength larger than 1300 nm. Moving to a shorter wavelength, the insertion loss will be increased but the extinction ratio will be enhanced. For the demonstrated 30 nm wavelength window, this hybrid silicon modulator can give a static extinction ratio from 10 dB to 20 dB with a 2 V bias change.

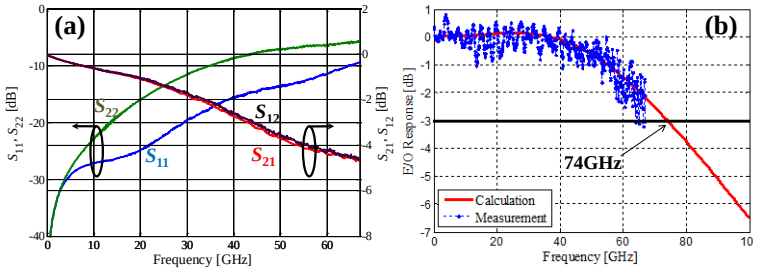

Fig. 5. (a) Measured scattering parameters of the segmented electrode; (b) the measured and calculated modulation responses.

Figure 5(a) shows the measured scattering parameters of the asymmetric segmented electrode. This measurement is calibrated to the probe tips of both the input and the output. We can see that the electrical reflection to the RF source (S_{11}) is less than −10 dB for the range from DC to 65 GHz. It indicates that the input impedance at the input port has been raised to 50 Ω and a wideband impedance matching has been reached by our design. Note that the difference of the S_{11} and S_{22} is due to the asymmetric configuration. The transmission (S_{21}

#165067 - $15.00 USD Received 21 Mar 2012; revised 26 Apr 2012; accepted 26 Apr 2012; published 4 May 2012

or S_{12}) shows a drop of 4.5 dB at 67 GHz, mainly from the microwave loss of the active segment and the long CPW on the output side.

The small-signal modulation of the HSEAM was measured by using a lightwave component analyzer (LCA, Agilent N4373C), where a GSG probe capped with a DC block and a standard 50 Ω off-chip terminator was attached to the output port of the device. Figure 5(b) shows the measured electro/optical (E/O) modulation response. Only a 2 dB drop has been observed up to 67 GHz, which is the upper limit of our LCA. The extrapolation based on simulation (assuming an intrinsic RC time constant of 1.3 ps) gives a 3 dB bandwidth of ~74 GHz. With such a large bandwidth, theoretically this device is able to support a non-return-to-zero (NRZ) transmission bit rate close to 100 Gb/s.

The large signal transmissions at a bit rate of 25 Gb/s, 40 Gb/s and 50 Gb/s were carried out on a device under a bias of −4 V. 2^{31}-1 NRZ pseudorandom bit sequence (PRBS) patterns were amplified to a level of around 2.2 Vpp and applied to the modulator. The eye diagrams of the drive signal after an additional 15 dB attenuator are shown in Fig. 6(a). For the measurement, the input wavelength was set at 1300 nm and the optical power reaching the modulator is around 4 dBm. A semiconductor optical amplifier, as well as a 1 nm bandpass optical filter, was inserted after the modulator to compensate the fiber-to-chip coupling loss. Figure 6(b) and Fig. 6(c) show the eye diagrams measured by a 53 GHz photoreceiver module (Agilent 86116A) in a digital communication analyzer for the back-to-back (B2B) transmission and a 16 km tranmisssion through a single mode fiber (SMF), respectively. All of these eye diagrams are very open, presenting more than 9 dB dynamic extinction ratios. Thanks to the low dispersion of the fiber at 1300 nm, no obvious degradation of the extintion ratio has been observed when the signal is delivered through the 16 km SMF. The reduction of the eye height is due to the loss of the SMF and the difference of the scale.

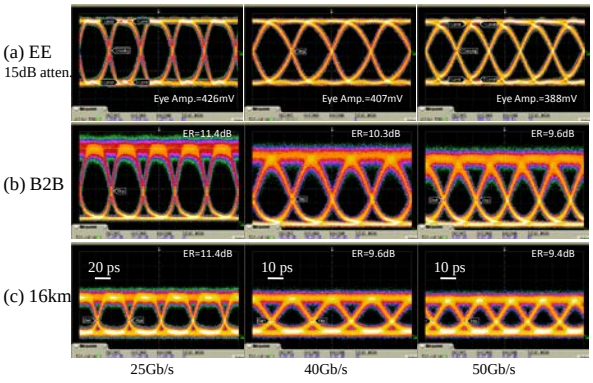

Fig. 6. Measured 2^{31}-1 PRBS NRZ eye diagrams at 25 Gb/s, 40 Gb/s and 50 Gb/s for (a) 15 dB attenuated drive signal, (b) back to back optical signal and (c) optical signal after 16 km tranmssion. The modulator under test was biased at −4 V with an input wavelength at 1300 nm.

Assuming a square pattern input, the power consumption (P) for this distributed modulator can be calculated by:

$$P \times B = \frac{1}{4}\frac{V_{\text{pp}}^2}{Z_{\text{in}}} + I_{\text{average}} V_{\text{bias}}, \quad (1)$$

The first item presents the extracted RF power from the source where V_{pp} and Z_{in} are the drive voltage swing and the input impedance at the input port of the modulator, respectively; The second item denotes the DC power consumption, where V_{bias} is the bias voltage and I_{average} is the averaged DC current during the measurement; B is the transmission bit rate. For the large signal measurement shown above, the current is around 1.55 mA, mostly coming from the photocurrent, Z_{in} is around 50 Ω and the V_{pp} is 2.2 V at 50 Gb/s. The power consumption at 50 Gb/s is around 608 fJ/bit for this HSEAM during the measurement.

#165067 - $15.00 USD Received 21 Mar 2012; revised 26 Apr 2012; accepted 26 Apr 2012; published 4 May 2012

4. Conclusions

In summary, we have demonstrated a 1.3 μm distributed III-V-on-Si electroabsorption modulator based on the hybrid silicon platform. The improved performance arises mainly from the new quantum well design and the asymmetric segmented electrode design. The measured E/O response shows a 2 dB drop at 67 GHz and an extrapolated 3 dB bandwidth of 74 GHz. Large signal measurements show clearly open eye diagrams with an extinction ratio of 9.6 dB for the back to back measurement and an extinction ratio of 9.4 dB after 16 km transmission at 50 Gb/s. These are the fastest modulators on silicon substrate demonstrated to date and the performance is similar to the best modulators on InP substrates.

Acknowledgments

This work was supported by the DARPA MTO EPHI program. The authors thank Scott Rodgers, Urban Westergren, Daoxin Dai, Doug Baney, Hui-Wen Chen, Siddharth Jain, Daryl Spencer, Ling Liao and Matthew N. Sysak for useful discussions and help.

#165067 - $15.00 USD Received 21 Mar 2012; revised 26 Apr 2012; accepted 26 Apr 2012; published 4 May 2012